Environmental Science and Pollution Research (2019) 26:10387–10397
https://doi.org/10.1007/s11356-019-04459-w

RESEARCH ARTICLE

The adsorption behavior of multiple contaminants like heavy metal ions and p-nitrophenol on organic-modified montmorillonite

Yawei Liu[1] · Jingde Luan[1] · Chengyu Zhang[1] · Xin Ke[1] · Haijun Zhang[1]

Received: 29 November 2018 / Accepted: 3 February 2019 / Published online: 14 February 2019

Abstract

Stearyl trimethyl ammonium chloride (STAC) and ethylenediamine (En) were successfully implanted into montmorillonite (MMt) interlayer to fabricate the novel adsorbent STAC-En-MMt for the simultaneous adsorption of Cu^{2+}, Zn^{2+}, and p-nitrophenol (PNP). X-ray diffraction, Fourier transform infrared spectroscopy, scanning electron microscopy, elemental analyzer, zeta potential analyzer, inductively coupled plasma mass spectrometry, and UV–visible spectrophotometer were used to investigate the microstructure characteristics of STAC-En-MMt and their adsorption capacity of target contaminants. Four factors such as pH, the molar ratio between En and STAC ($R_{En/STAC}$), the adsorption time (A_{Time}), and the adsorption temperature (A_{Temp}) were selected to investigate the adsorption capacities of Cu^{2+}, Zn^{2+}, and PNP onto STAC-En-MMt in ternary solution. The results indicated that the total simultaneous adsorption of Cu^{2+}, Zn^{2+}, and PNP onto STAC-En-MMt adsorbent with $R_{En/STAC} = 0.75$ reached up to 260.27 mmol·kg^{-1} under the condition of pH = 6, $A_{Temp} = 40$ °C, and $A_{Time} = 60$ min. After three regenerations, there was still a good performance in the adsorption of STAC-En-MMt. The Langmuir adsorption isotherm indicated that the adsorption of heavy metals and PNP onto adsorbents were single-layer surface adsorption. Nonlinear adsorption kinetics simulation indicated that chemical adsorption occupied a predominant position in Cu^{2+} and Zn^{2+} adsorption, while PNP adsorption depended on physical adsorption. Compared with Zn^{2+}, Cu^{2+} had higher affinity for the adsorption sites on STAC-En-MMt. However, the pore blocking caused by the Cu^{2+} and Zn^{2+} adsorption had a remarkably adverse effect on PNP adsorption.

Keywords Montmorillonite · Organic combinated modification · Adsorption behavior · Multiple contaminants

Introduction

Environmental pollution is a serious challenge to the sustainable economic development in the world, especially industrial sewage discharge. For a long time, water pollution control engineering research mostly focuses on the treatment of single organic contaminants or heavy metals, but in the actual water environment, organic contaminants and heavy metals are not completely separated, but coexist in the same pollution source or environment. For example, printing and dyeing wastewater is a typical industrial wastewater with combined pollution of refractory organic matter and heavy metal ions. Untreated printing and dyeing wastewater contains not only a large number of toxic dyes, but also Cu^{2+}, Zn^{2+}, and other heavy metal elements (Wang et al. 2008; Ying and Liu 2014). There are also various types of contaminants in refinery wastewater: heavy metals such as zinc and chromium, polycyclic aromatic hydrocarbons, ammonium salts, sulfides, cyanides, phenols (Hamidian et al. 2014; Li et al. 2015). Therefore, how to simultaneously remove organic matter and heavy metals from wastewater economically and effectively has become an important issue in the field of environmental protection in recent years. Among sewage treatment technologies, adsorption is considered as the most convenient method for the removal of heavy metal ions and organic contaminants due to low cost

Responsible editor: Tito Roberto Cadaval Jr

✉ Jingde Luan
jdluan@sau.edu.cn

[1] College of Energy and Environment, Shenyang Aerospace University, 37 Daoyi South Street, Shenyang 110136, People's Republic of China

implementation and high removal efficiency (Ennigrou et al. 2014; Hua et al. 2012; Jin et al. 2017; Zhang et al. 2018b).

Mineral adsorbents have become an alternative of activated carbon and have been applied to sewage treatment (Awadallah-F and Naguib 2017; Dashairya et al. 2018; Nicolás et al. 2016; Wang et al. 2017; Yu et al. 2018). As a kind of clay minerals, montmorillonite (MMt) has advantage in the changeable layer spacing, domain charge, and medium environment (Pawar et al. 2016; Zhang et al. 2018a). Through single organic modification, the natural interlayer hydrophilic environment of MMt was converted to hydrophobic environment, which provides a convenient condition for organic contaminants adsorption. Meanwhile, the intercalation of organic modifier can enhance the adsorption capacity of heavy metal ions like Pb^{2+} and Cr^{3+} due to their coordination complex reaction (Hu et al. 2016; Wang et al. 2011; Zhu et al. 2016). However, the hydrophobic interlayer environment has a negative impact on the adsorption of heavy metals onto MMt. Moreover, this intercalation has an adverse effect on the adsorption capacity of organic contaminants due to their high stacking density of organic modifier in MMt interlayer (Zhou et al. 2015).

The complex modification technologies provide an effective method to avoid the reduction in the adsorption capacity of heavy metal ions onto MMt by single organic modification. When MnO and polymethylene diallyl ammonium chloride were continuously intercalated into MMt interlayer, there was a positive effect on As adsorption due to the increase in specific surface area and pore volume of the complex–modification MMt (Hua 2015). When Fe polycations and cetyltrimethylammonium bromide (CTMAB) were adopted to prepare the modified MMt, it was found that CTMAB was intercalated into MMt interlayer while Fe polycations was attached to MMt surface, which exhibited better adsorption for heavy metal cations (Ren et al. 2014). Actually, the surface electronegativity of nature MMt is a barrier to the effective adsorption of anionic contaminants. If heavy metal cations and anionic organic contaminants exist in sewage, it is necessary to find a new synthetic method of modified MMt to achieve efficient adsorption.

Stearyl trimethyl ammonium chloride (STAC) can create a hydrophobic environment in MMt interlayer for the adsorption of organics. Ethylenediamine (En) can improve the adsorption of organic contaminants onto MMt by introducing carboxyl, amino, and chlorine functional groups (Dong et al. 2010; Zhu et al. 2010). In our study, both STAC and En were adopted to fabricate the organic synthetic adsorbent STAC-En-MMt for the simultaneous adsorption of Cu^{2+}, Zn^{2+}, and p-nitrophenol (PNP), revealing the adsorption behavior of inorganic and organic contaminants and their competitive adsorption mechanism.

Materials and methods

Materials

Nature Na-MMt (CEC = 0.95 mol·kg^{-1}) powder was purchased from Gongyi, Henan province, China. Experimental reagents like STAC, En, HCl, NaOH, anhydrous ethanol, the standard solution of $Cu(NO_3)_2$, $Zn(NO_3)_2$, and PNP were purchased from Sinopharm Chemical Reagent Co., Ltd. (Shenyang city, China). Deionized water was used in test solution preparation and container cleaning.

Preparation of organic-modified MMt

Five grams of purified Na-MMt powder was dispersed in 200 mL deionized water, which was placed in a 400-mL three-mouth flask. Then, 2 g STAC was added into this suspension to prepare the organic-modified MMt (STAC-MMt) by ultrasonic stirring for 20 min, then continuous mechanical stirring at 250 r/min for 120 min. In the preparation process of organic-modified MMt, the modifier En was introduced to change the mole ratios of En and STAC ($R_{En/STAC}$) in order to produce STAC-En-MMt samples. The vacuum filtration was adopted to obtain the filter cake, which was washed with anhydrous ethanol and deionized water for three times, respectively. Through drying at 90 °C in air circulation oven for 24 h, the prepared organic-modified MMt samples were cooled at room temperature and then were crushed into powder for adsorption experiments.

Characterization

Inductively coupled plasma mass spectrometry (Optima-PE8300, PE, USA) was adopted to measure Cu^{2+} and Zn^{2+} concentration, while UV–visible spectrophotometer (UNIC-uv-2100, Shanghai) was introduced to determine PNP concentration by the absorbance value at wavelength of 317 nm. The specific surface area, pore size, and pore volume of the experimental samples were confirmed by the fully automated physical adsorption instrument (Autosorb iQ-C, Quantachrome Instruments, USA). Mineral composition analysis was carried out at X-ray diffractometer (7000S, Shimadzu, Japan) at the scanning speed 2°/min and in the scanning range between 2 and 60°. The change in the functional groups of testing samples was analyzed by the infrared spectrometer (Nicolet iN10 MX and iS10, Thermo Fisher, USA) at spectrum of 600–4000 cm^{-1}. The scanning electron microscopy (FEI-Nova NanoSEM 450, USA) was adopted to observe the changes in microstructure of experimental samples. The changes in elemental composition and potential of testing samples were analyzed by Elemental Analyzer (Vario EL cube, Ellimonta, Germany) and Zeta Potential Analyzer (Zetasizer Nano ZS, Malvern, British).

Adsorption experiments and modeling

Adsorption experiments

Half gram of experimental powder of prepared organic-modified MMt was placed in a conical flask containing 20 mL solution prepared by Cu^{2+}, Zn^{2+}, and PNP (100 mg/L). Adsorption experiments were performed by batch technique in a temperature-controlled shaker to investigate the effect of pH (2, 3, 4, 5, 6), $R_{En/STAC}$ (0.25, 0.5, 0.75, 1.00, 1.25), the adsorption time (A_{Time} = 30, 60, 90, 120, 150 min), and adsorption temperature (A_{Temp} = 20, 30, 40, 50, 60 °C) on the co-adsorption behavior of Cu^{2+}, Zn^{2+}, and PNP.

The adsorption capacity (Q) of three contaminants were calculated using the following equations:

$$Q = \frac{(C_o - C_e)V}{M \cdot m} \quad (1)$$

where Q is the amount of adsorbate (Cu^{2+}, Zn^{2+}, and PNP) adsorbed on the adsorbent at equilibrium (mmol/kg), C_o and C_e are the initial and equilibrium concentrations of adsorbate (g/L), V is the volume of the aqueous solution containing Cu^{2+}, Zn^{2+}, and PNP (L), M is the molar mass of adsorbent (kg/mol), m is the weight of adsorbent used in the experiments (kg).

Adsorption isotherms

The Langmuir and Freundlich adsorption isotherms were adopted to predict the saturated adsorption capacity of the adsorbent under best adsorption conditions, as described in Eqs. (2) and (3)

$$q_e = \frac{q_{max} K_L C_e}{1 + K_L C_e} \quad (2)$$

$$q_e = K_F C_e^{\frac{1}{n}} \quad (3)$$

where C_e (mg/L) and q_e (mmol/kg) are the concentrations of target contaminants in the solution after equilibrium and the amount of target contaminants onto adsorbent, respectively. K_L (L/mg) is the Langmuir adsorption constant, and K_F (mg/g) is the Freundlich adsorption constant. q_{max} (mmol/kg) is the saturated adsorption capacity.

Adsorption kinetics

Pseudo-first-order (4), pseudo-second order (5), and particle internal diffusion model (6) were adopted to investigate the adsorption behavior of target contaminants onto organic-modified MMt in adsorption process. The specific expressions are as follows:

$$q_t = q_e[1 - \exp(-k_1 t)] \quad (4)$$

$$q_t = \frac{q_e^2 k_2 t}{1 + k_2 q_e t} \quad (5)$$

$$q_t = K_p\left(t^{\frac{1}{2}}\right) + C \quad (6)$$

q_e and q_t (mmol/kg) are the adsorption quantities of target contaminants at equilibrium, and in any contact time, respectively. k_1 and k_2 are the equilibrium rate constants of two kinetic models, respectively. K_p is the internal diffusion rate constant, while C is the y-intercept at some stage.

Results and discussions

Structural characterization

XRD analysis

Layer spacing is the most important structural information in the internal structure characteristics of modified MMt, and it is also an important parameter to judge the effect of modification on their adsorption capacities. According to the famous Bragg's law, the distance between layers can be calculated by its diffraction peak. The XRD analysis (Fig. 1) indicated that nature MMt just had a weaker diffraction peak at 2θ = 8.6° with a distance of 0.955 nm. However, when STAC and En was introduced into MMt interlayer, a strong diffraction peak appeared in STAC-MMt and STAC-En-MMt, and their interlayer spacing increased to 2.068 nm and 2.117 nm, respectively.

BET analysis

N_2 adsorption–desorption curve distributions of MMt before and after organic modification (Fig. 2) indicated that MMt,

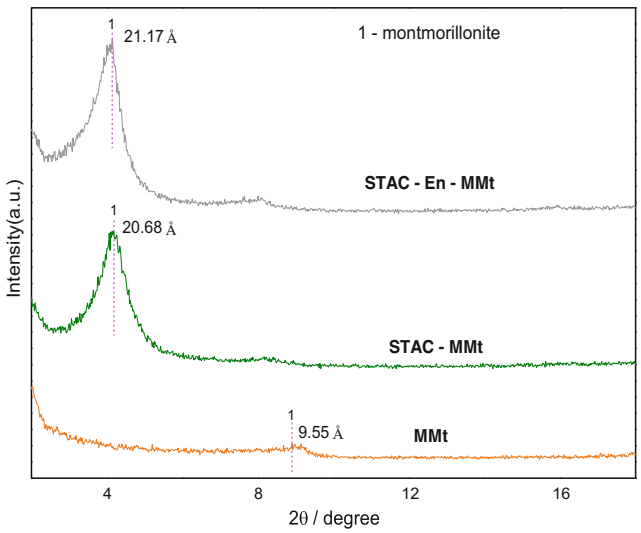

Fig. 1 XRD patterns of MMt and organic-modified MMt

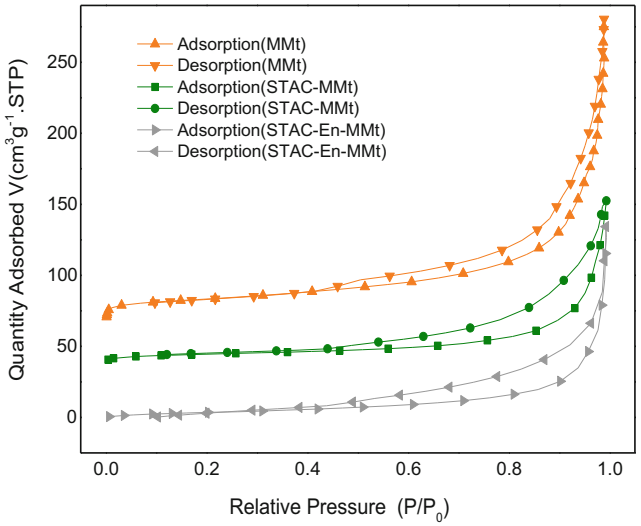

Fig. 2 N_2 adsorption–desorption curve distributions of MMt, STAC-MMt, and STAC-En-MMt

STAC-MMt, and STAC-En-MMt belong to the typical type IV isotherm, while there are H3 hysteresis loops, indicating that all three materials have mesopore structure (Long et al. 2013). In the preparation process of STAC-MMt and STAC-En-MMt, there was a remarkable reduction in the specific surface area from 49.31 m^2/g of nature MMt to 17.54 m^2/g and 15.47 m^2/g, respectively (Table 1). The pore volume and pore size of STAC-MMt reduced from 0.314 cm^3/g and 17.011 nm of nature MMt to 0.168 cm^3/g and 14.652 nm, respectively. This phenomenon indicated that STAC entered into MMt interlayer, and partial STAC caused the pores blocked. When En was implanted into the interlayer of STAC-MMt, some of STAC macromolecules were replaced by En, which slowed down the blocking effect of pores. Therefore, there was a slight improvement in the pore volume and pore size of STAC-En-MMt.

Elemental analysis

Elemental analysis indicated that there was trace amount of carbon (C) in nature MMt though the nitrogen was nil (Table 2). When STAC ($C_{21}H_{46}ClN$) and En ($C_2H_8N_2$) were intercalated into MMt interlayer, there would absolutely be a significant change in the content of N and C. Table 2 showed that the N and C contents of STAC-MMt were about 2.15 wt% and 26.14 wt%, respectively. When En was implanted into STAC-MMt, STAC-En-MMt had an increase in N and C contents due to the substitution reaction of STAC macromolecules.

Table 1 BET analysis of MMt, STAC-MMt, and STAC-En-MMt

Parameter	Three adsorbents		
	MMt	STAC-MMt	STAC-En-MMt
BET surface area (m^2/g)	49.31	17.54	15.47
Pore volume (cm^3/g)	0.314	0.168	0.202
Pore size (nm)	17.011	14.652	15.503

Table 2 Element analysis of organic phase in MMt, STAC-MMt, and STAC-En-MMt

Elemental	Material (wt%)		
	MMt	STAC-MMt	STAC-En-MMt
N	0	2.15	2.46
C	2.01	26.14	27.33
C/N	–	12.16	11.11

FTIR analysis

FTIR analysis (Fig. 3) indicated that the functional group of STAC-MMt and STAC-En-MMt undergone a dramatic change. There was an increase in the CH symmetric stretching vibration absorption peak at the wave number of 2853 cm^{-1}. Meanwhile, another peak appeared at 2917 cm^{-1} attributed to the $-CH_2$ antisymmetric stretching vibration. The OH stretching absorption peak at the wave number of 3444 cm^{-1} was reduced significantly due to the exchange of quaternary ammonium cations with interlaminar water molecules (Long et al. 2013). The analysis of STAC-En-MMt after adsorption confirmed that the intensity of the OH stretching vibration peak at wavenumber of 3444 cm^{-1} was further weakened, and a new absorption peak appeared at 1382 cm^{-1}, indicating that the adsorbed Cu^{2+} and Zn^{2+} combined with En in MMt interlayer to form a stable complex (Yu et al. 2010).

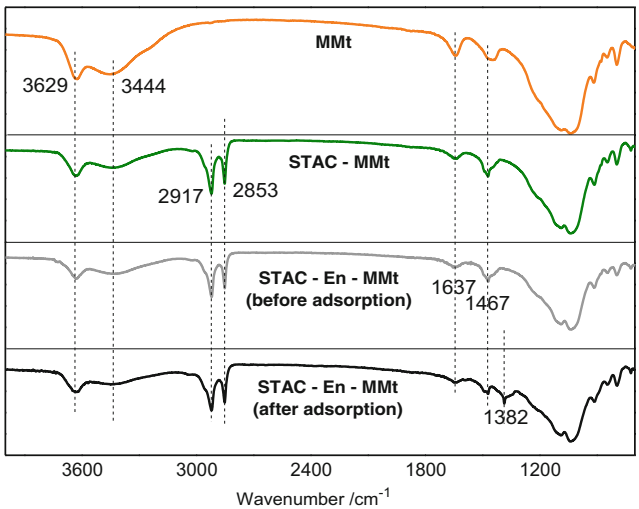

Fig. 3 FTIR patterns of experimental sample before and after adsorbing Cu^{2+}, Zn^{2+}, and PNP

Microstructure analysis

SEM analysis indicated that there was a remarkable difference in the microstructure of experimental samples prepared by different modification methods. Though there were a large number of irregular fragments in MMt (Fig. 4a), the large blocks appeared in the microstructure of modified MMt due to the aggregation effect by the intercalation of STAC and En (Fig. 4b, c). After adsorbing the adsorption of Cu^{2+}, Zn^{2+}, and PNP, the honeycomb structure appeared on the surface of STAC-En-MMt (Fig. 4d).

Adsorption performance of modified MMt

Effect of pH value

pH is an important factor on affecting the adsorption process. This study found that Cu^{2+} and Zn^{2+} was precipitated as hydroxides when pH value exceeded 6.5. The prepared STAC-En-MMt sample was adopted to carry out the co-adsorption of Cu^{2+}, Zn^{2+}, and PNP under the condition of $R_{En/STAC} = 1$, $A_{Time} = 120$ min, and $A_{Temp} = 30$ °C (Fig. 5) to investigate the effect of pH value on its adsorption behavior. When the pH value increased from 2 to 6, the adsorption capacity of Cu^{2+} onto STAC-En-MMt increased from 15.44 mmol·kg^{-1} to 154.11 mmol·kg^{-1}, while that of Zn^{2+} increased from 8.86 mmol·kg^{-1} to 29.01 mmol·kg^{-1}. This phenomenon was the reason in that the competition of H^+ was better than heavy metal ions to adsorption sites at lower pH. The adsorption capacity of PNP onto STAC-En-MMt increased from 43.06 to 69.24 mmol·kg^{-1}. This could be attributed to the enhancement of hydrophobicity of STAC-En-MMt as the pH increase (Fig. 5).

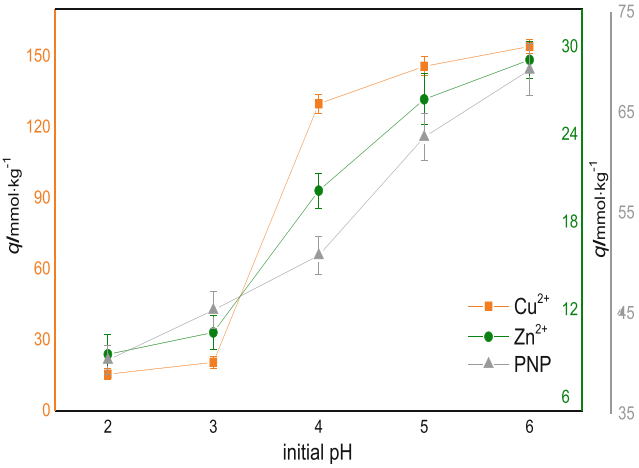

Fig. 5 Effect of pH on the adsorption properties of Cu^{2+}, Zn^{2+}, and PNP by STAC-En-MMt

$R_{En/STAC}$ effect (pH = 6, A_{Time} = 120 min, A_{Temp} = 30 °C)

When $R_{En/STAC} = 0.75$, the adsorption of Cu^{2+} and Zn^{2+} onto STAC-En-MMt samples reached the maximum, which were 158.91 mmol·kg^{-1} and 32.35 mmol·kg^{-1}, respectively

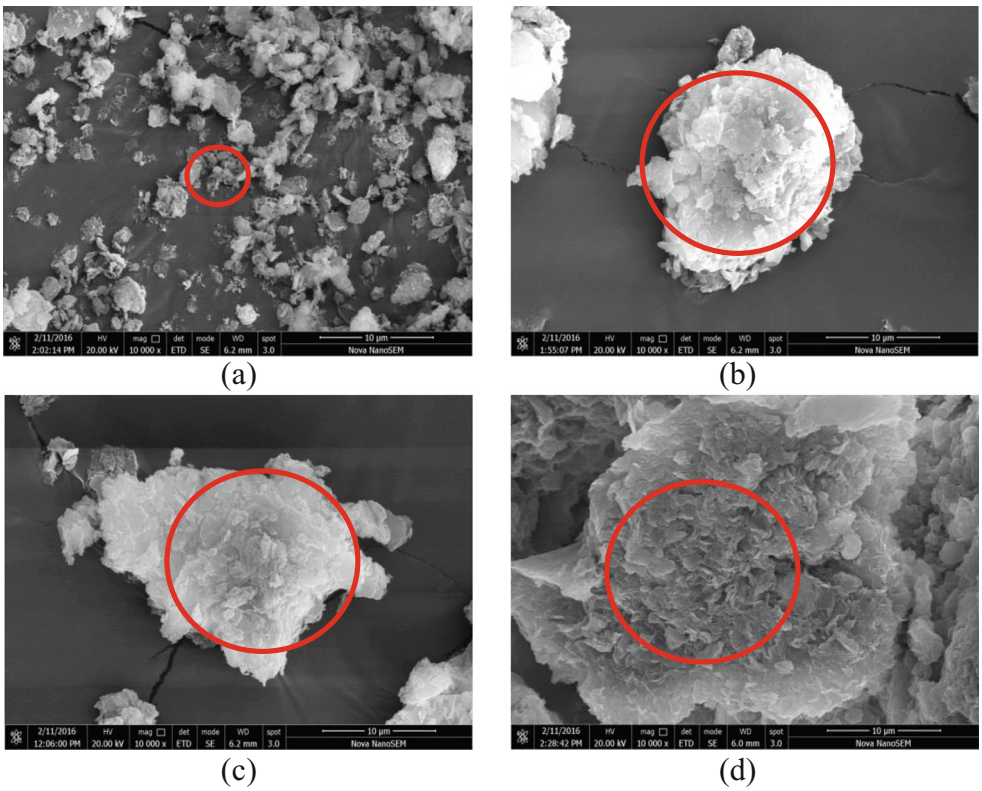

Fig. 4 Microstructure of experimental sample: (**a**) nature MMt. **b** STAC-MMt. **c** STAC-En-MMt. **d** STAC-En-MMt adsorbing Cu^{2+}, Zn^{2+}, and PNP

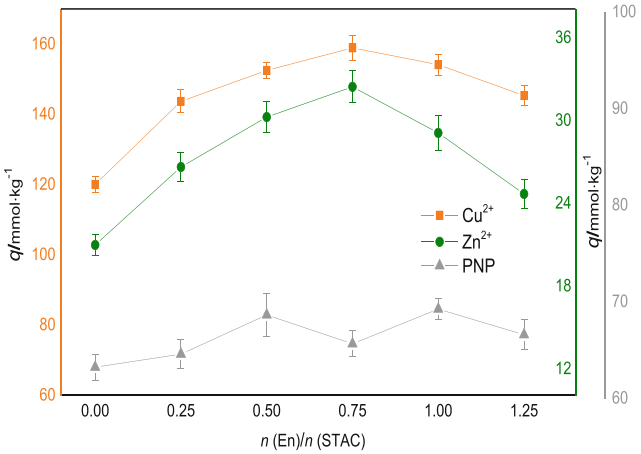

Fig. 6 Effect of $R_{En/STAC}$ on the adsorption properties of Cu^{2+}, Zn^{2+}, and PNP by STAC-En-MMt

(Fig. 6). When $R_{En/STAC} > 0.75$, there was an obvious decrease in the adsorption quantities of Cu^{2+} and Zn^{2+} onto STAC-En-MMt due to the pores blocking caused by excess En, which led to the inability of Cu^{2+} and Zn^{2+} to enter the interlayer through the pores. Although the intercalation of En had a significant effect on the adsorption quantities of heavy metal ions onto STAC-En-MMt, PNP adsorption fluctuated within a small range of 60–70 mmol·kg^{-1}. Based on the above, STAC-En-MMt sample with $R_{En/STAC} = 0.75$ was adopted to carry out the following research due to the total adsorption maximum of target contaminants about 256.9 mmol·kg^{-1}.

Effect of contact time (pH = 6, $R_{En/STAC}$ = 0.75, A_{Temp} = 30 °C)

The effect of contact time on the adsorption behavior of STAC-En-MMt was investigated under the condition of $A_{Temp} = 30$ °C, pH = 6, and R_{En}/STAC = 0.75. The adsorption quantity of PNP on STAC-En-MMt was closed to the maximum value of 65.73 mmol·kg^{-1}, indicating that PNP adsorption equilibrium was achieved within 30 min (Fig. 7). When the adsorption time increased to 60 min, the adsorption equilibrium of Cu^{2+} and Zn^{2+} onto STAC-En-MMt was achieved, and their adsorption capacities were about 159 mmol·kg^{-1} and 32 mmol·kg^{-1}, respectively. With a view to the simultaneous adsorption of heavy metal ions and PNP, the optimum adsorption time was considered as 60 min.

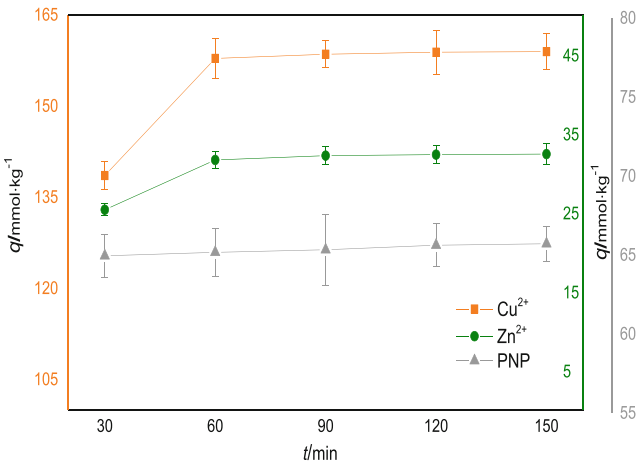

Fig. 7 Effect of A_{Time} on the adsorption properties of Cu^{2+}, Zn^{2+}, and PNP by STAC-En-MMt

Effect of temperature (pH = 6, $R_{En/STAC}$ = 0.75, A_{Time} = 60 min)

Figure 8 indicated that there was a positive effect of temperature on the adsorption quantities of heavy metal ions, but the increase of temperature had an adverse effect on PNP adsorption. The corresponding adsorption capacities of Cu^{2+}, Zn^{2+}, and PNP onto STAC-En-MMt were 174.53 mmol·kg^{-1}, 37.15 mmol·kg^{-1}, and 48.59 mmol·kg^{-1}, respectively. Therefore, the total co-adsorption quantity of Cu^{2+}, Zn^{2+}, and PNP added up to 260.27 mmol·kg^{-1}. Although there was a weak improvement of STAC-En-MMt adsorption capacities to Cu^{2+} and Zn^{2+} with the increase of adsorption temperature, the total co-adsorption quantity of target contaminants was continuously decreasing.

Synchronous adsorption of target contaminants on three adsorbents

The Langmuir and Freundlich sorption isotherms of MMt, STAC-MMt, and STAC-En-MMt ($R_{En/STAC} = 0.75$) were plotted under the best adsorption conditions (Fig. 9). By comparison, it was found the Langmuir adsorption isotherm could describe the adsorption process more accurately due to the higher fitting correlation coefficient, which indicated that the adsorption of heavy metals and PNP by adsorbents were single-layer surface adsorption (Table 3). When STAC was implanted into MMt interlayer, there was a downward trend in the adsorption capacities of Cu^{2+} and Zn^{2+} onto STAC-

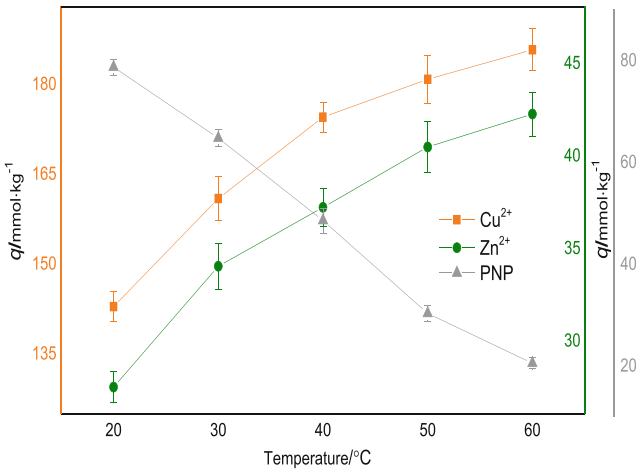

Fig. 8 Effect of A_{Temp} on the adsorption properties of Cu^{2+}, Zn^{2+}, and PNP by STAC-En-MMt

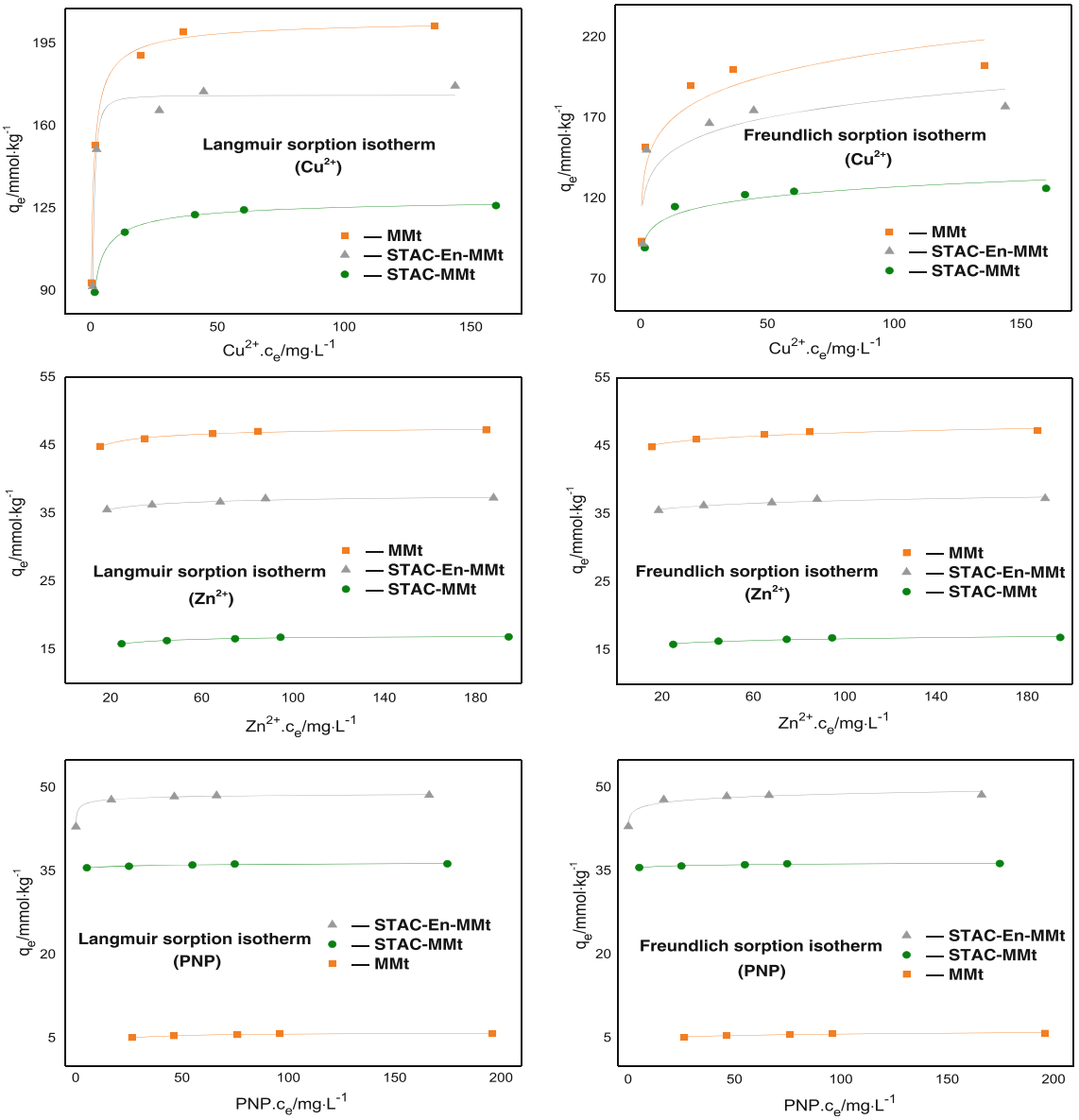

Fig. 9 Langmuir and Freundlich sorption isotherm analysis on three adsorbents for the adsorption capacities of Cu^{2+}, Zn^{2+}, and PNP

Table 3 Parameters of adsorption isotherms of different materials

		Langmuir model			Freundlich model		
Adsorbate	adsorbent	q_{max} (mmol/kg)	K_L	R_L^2	K_F	$1/n$	R_F^2
Cu^{2+}	MMt	205.80	1.80	0.996	129.27	0.11	0.816
	STAC-MMt	130.50	1.62	0.998	90.85	0.07	0.869
	STAC-En-MMt	172.96	1.49	0.978	117.90	0.09	0.658
Zn^{2+}	MMt	47.94	2.32	0.977	42.47	0.02	0.899
	STAC-MMt	17.06	0.62	0.966	14.44	0.03	0.864
	STAC-En-MMt	38.21	2.96	0.935	33.44	0.02	0.911
PNP	MMt	6.00	0.21	0.958	4.17	0.07	0.857
	STAC-MMt	43.34	4.32	0.942	35.23	0.01	0.912
	STAC-En-MMt	49.70	11.67	0.997	44.90	0.02	0.954

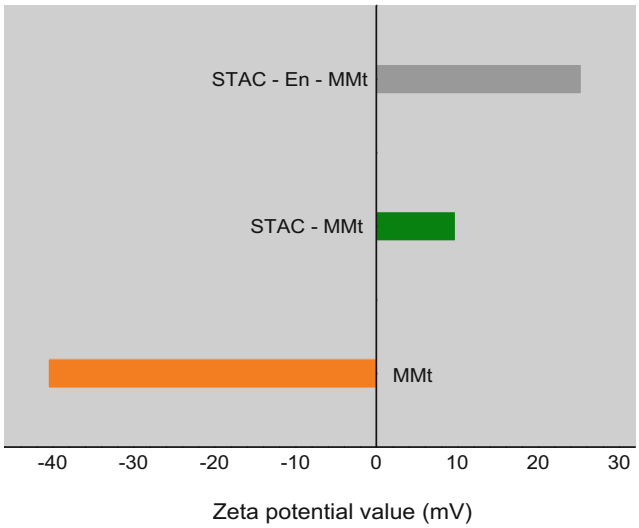

Fig. 10 Zeta potential values of three adsorbents

MMt due to the changed interlayer environment of montmorillonite from hydrophilic to hydrophobic.

However, the implantation of En provided new chelation sites for heavy metal ions, which significantly increased the adsorption capacities of target ions. Moreover, the adsorption capacity of heavy metal ions was also related to pore size and pore volume of STAC-En-MMt sample based on N_2 adsorption–desorption results. The adsorption capacity of PNP onto mineral adsorbents was mainly related to the organic phase content, and the relative values of MMt, STAC-MMt, and STAC-En-MMt were 6.00 mmol·kg^{-1}, 43.34 mmol·kg^{-1}, and 49.70 mmol·kg^{-1}, respectively. The elemental analysis of three adsorbents indicated that the implantation of STAC and En increased the content of organic carbon and organic nitrogen in montmorillonite. The total adsorption capacity of Cu^{2+}, Zn^{2+}, and PNP onto STAC-En-MMt sample added up to 260.87 mmol·kg^{-1}, which was the maximum adsorption capacity of three adsorbents.

Adsorption mechanism analysis

There are three adsorption modes of heavy metal ions on clay mineral adsorbents: electrostatic attraction, ion exchange, and coordination complexes (Ijagbemi et al. 2009; Wu et al. 2012; Zhu et al. 2016). Electrostatic attraction is a physical adsorption reaction, but ion exchange and coordination

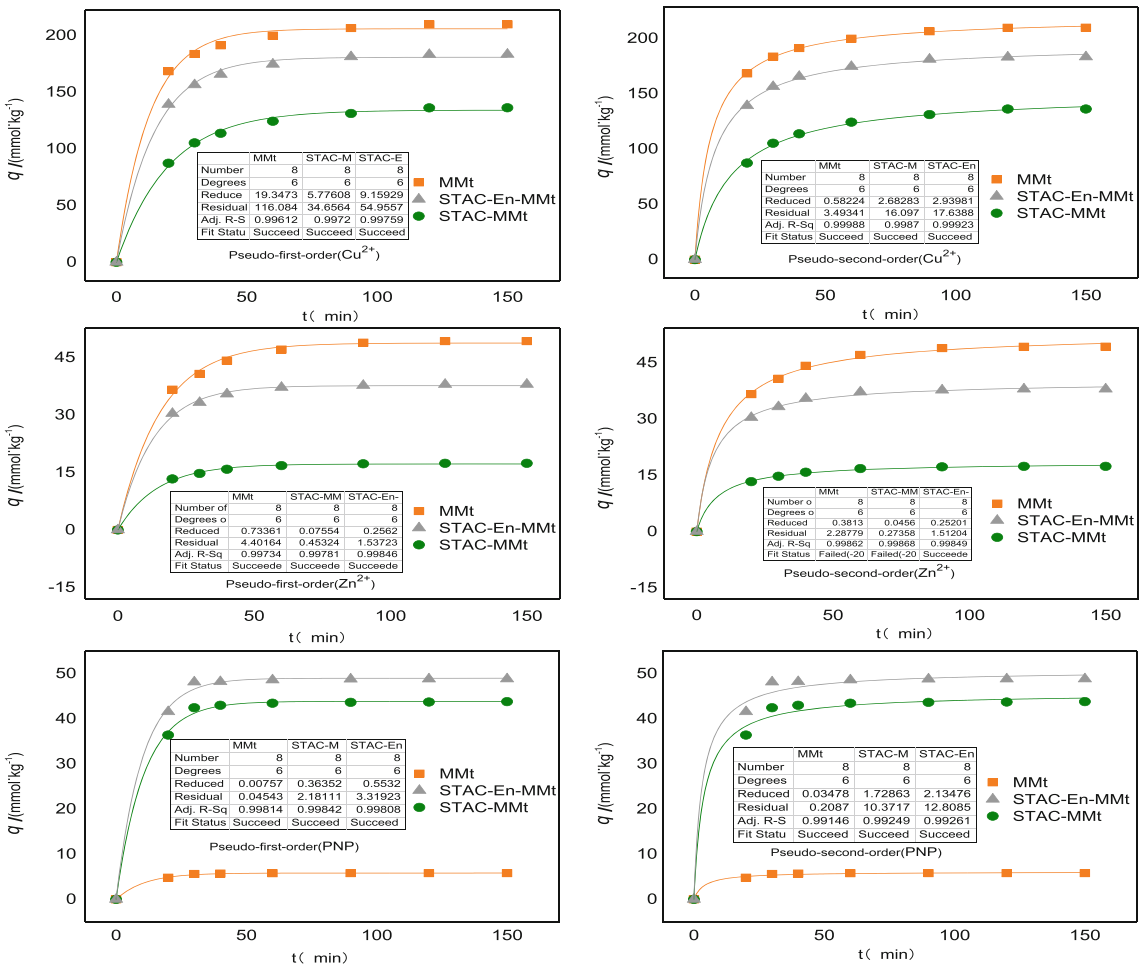

Fig. 11 The pseudo-first order and pseudo-second order plots of Cu^{2+}, Zn^{2+}, and PNP onto three adsorbents

complexation are chemical adsorption reactions. Zeta potential analysis confirmed that the surface charge of organic-modified MMt changed from negative to positive (Fig. 10), indicating that electrostatic attraction was already not one of the main adsorption modes for STAC-En-MMt. The FTIR analysis on STAC-En-MMt after adsorption showed that Cu^{2+} and Zn^{2+} combined with the chelation En to form a stable complex due to new absorption peak appeared at 1382 cm^{-1}, indicating that coordination complexes were in a predominant position in the adsorption behavior of heavy metal ions. Since MMt before and after modification contained the exchangeable cations Na^{+} and STA^{+}, ion exchange was also one of the main adsorption modes. Therefore, the main adsorption behavior of Cu^{2+} and Zn^{2+} onto STAC-En-MMt had an obvious transition from electrostatic attraction and ion exchange of nature MMt to ion exchange and coordination complexation.

The adsorption kinetic curves (Fig. 11) indicated that the pseudo-second order model exhibited a higher fitting degree to Cu^{2+} and Zn^{2+} adsorption due to higher *R*-square, which explained that chemical sorption was the main rate limiting step in the Cu^{2+} and Zn^{2+} adsorption process. However, the pseudo-first order model had a better fitting degree to PNP adsorption, demonstrating that physical adsorption was the main mode in PNP sorption process. The particle internal diffusion model (Fig. 12) showed that the linear part did not pass through the origin, indicating that intraparticle diffusion was not the only control step in the adsorption of heavy metals and PNP. The first stage could be attributed to the molecular diffusion of heavy metals and PNP from water to surface. The second stage showed that there were chemical reactions such as substance exchange during the diffusion of adsorbent particles. Furthermore, the particle internal diffusion of target contaminants onto adsorbent diminished gradually after the equilibrium of adsorption which indicated on the third stage. The analysis of the whole model showed that the adsorption process was mainly controlled by the diffusion of the molecular surface, followed by the internal diffusion.

The prepared mineral adsorbent STAC-En-MMt ($R_{En/STAC} = 0.75$) exhibited a good adsorption performance for Cu^{2+}, Zn^{2+}, and PNP (Fig. 13). The single adsorption capacities of Cu^{2+}, Zn^{2+}, and PNP on STAC-En-MMt were 212.45 mmol·kg^{-1}, 171.98 mmol·kg^{-1}, and 134.14 mmol·kg^{-1}, respectively. When STAC-En-MMt was adopted to carry out the simultaneous adsorption of target contaminants, the adsorption capacities of STAC-En-MMt for Cu^{2+}, Zn^{2+}, and PNP were 174.53 mmol·kg^{-1}, 37.15 mmol·kg^{-1}, and 48.59 mmol·kg^{-1}, respectively (Fig. 13). These results indicated that there was a remarkable reduction in the adsorption capacity and a significant competitive adsorption. Due to the chemical adsorption between heavy metal ions and STAC-En-MMt, it can be found that

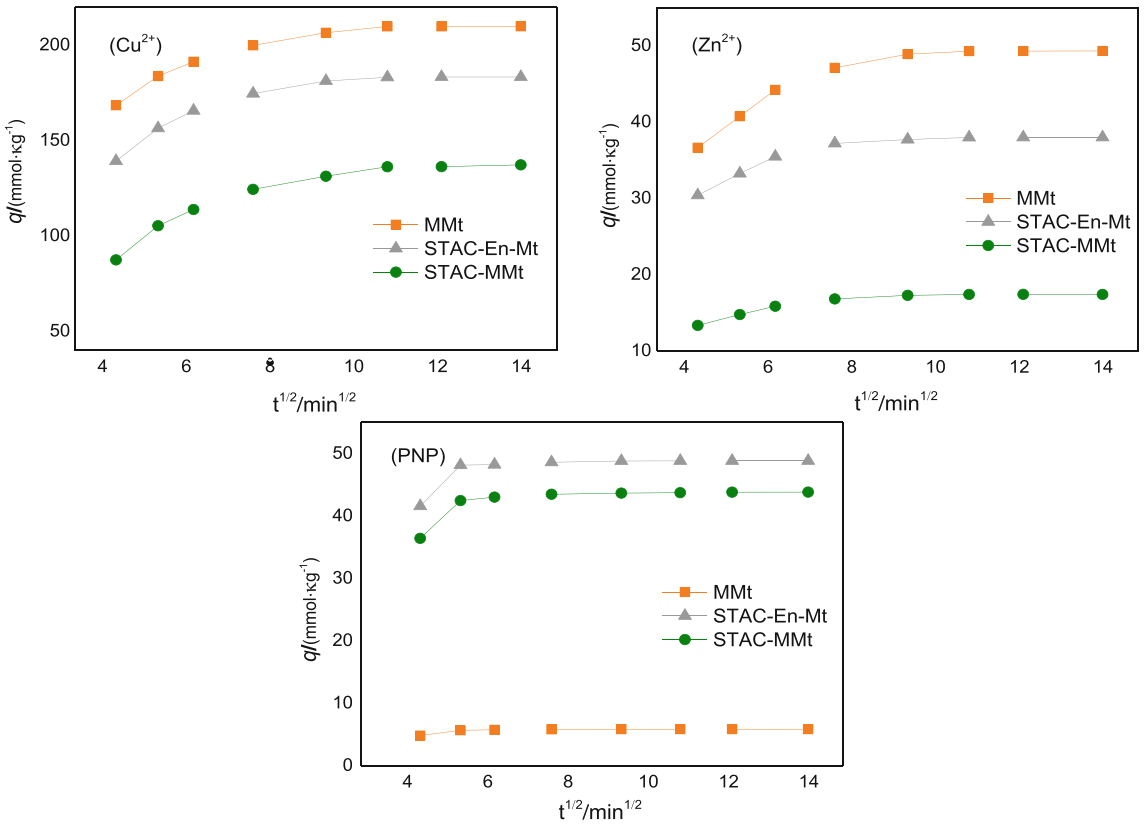

Fig. 12 The particle internal diffusion plots of Cu^{2+}, Zn^{2+}, and PNP onto three adsorbents

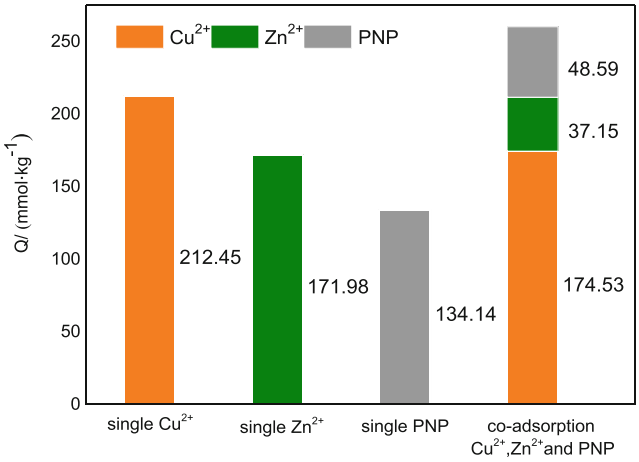

Fig. 13 Synchronization and single adsorption performance of STAC-En-MMt

there was an obvious priority for Cu^{2+} to compete the adsorptive sites with Zn^{2+}. The adsorption of Cu^{2+} and Zn^{2+} onto STAC-En-MMt caused a further exacerbation of the pore blocking, leading to a significant reduction in PNP adsorption.

Regeneration performance of STAC-En-MMt

To investigate the influence of the regeneration frequency on the adsorption capacity, STAC-En-MMt undergone desorption in the solution (0.5 mol·L^{-1} HCl) for 6 h and was calcined in a muffle furnace at 200 °C for 4 h. After multiple desorption and calcinations, there was a downward trend in the adsorption capacities of Cu^{2+} and Zn^{2+} onto STAC-En-MMt. However, the adsorption capacities of Cu^{2+} and Zn^{2+} on STAC-En-MMt through three regenerations still exceeded 150 mmol·kg^{-1} and 30 mmol·kg^{-1}, respectively (Fig. 14). The continuous regeneration reduced significantly the adsorption capacity of Cu^{2+} and Zn^{2+} due to the poor thermal stability of the chelating agent En. Though multiple calcinations

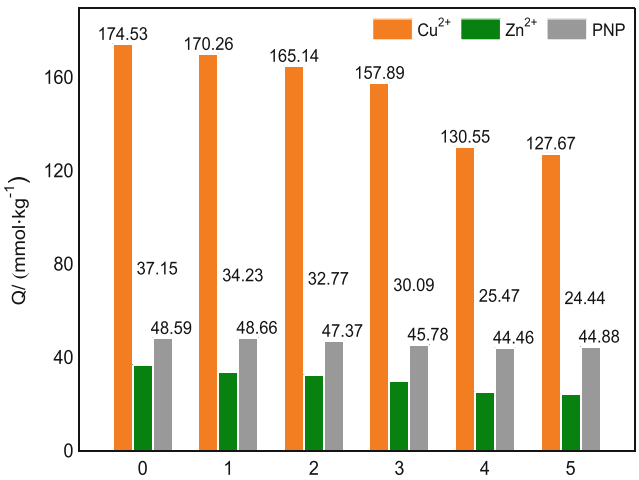

Fig. 14 Effect of regeneration times on the adsorption performance of STAC-En-MMt

destroyed the structure of En, it did not change the interlayer hydrophobicity. Therefore, PNP adsorption capacity on the regenerated STAC-En-MMt remained at a relatively high level.

Conclusions

The organic modifiers like STAC and En were implanted into MMt interlayer to prepare mineral adsorbent for the simultaneous adsorption of Cu^{2+}, Zn^{2+}, and PNP. Four factors such as pH, $R_{En/STAC}$, the adsorption time, and the adsorption temperature were selected to investigate the adsorption performance of MMt before and after modification. The results indicated that the simultaneous adsorption capacities of Cu^{2+}, Zn^{2+}, and PNP onto STAC-En-MMt ($R_{En/STAC} = 0.75$) were 174.53 mmol·kg^{-1}, 37.15 mmol·kg^{-1}, and 48.59 mmol·kg^{-1} under the condition of pH = 6, A_{Temp} = 40 °C, and A_{Time} = 60 min, respectively. Meanwhile, this was the maxim for the total simultaneous adsorption of target contaminants. Langmuir adsorption isotherm under the best adsorption conditions indicated that STAC-En-MMt had the largest total saturated adsorption capacity. The adsorption mechanism analysis indicated that there was a significant transition in the main adsorption mode of Cu^{2+} and Zn^{2+} onto MMt adsorbent from electrostatic attraction and ion exchange before modification to ion exchange and coordination complexation after organic modification. The pseudo-second order kinetic implied that chemical adsorption was predominant in the adsorption of heavy metal ions, while physical adsorption was good at elucidating PNP adsorption process based on the pseudo-first order kinetic. The particle internal diffusion model showed that the adsorption process was mainly controlled by the diffusion of the molecular surface, followed by the internal diffusion. Through three regenerations, there was still a good performance in the adsorption of target contaminants onto STAC-En-MMt.

Funding information This work was financially supported by Liaoning Provincial Natural Science Foundation of China (grant number 20180510024).

References

Awadallah-F A, Naguib HF (2017) Grafting of tea waste with polyacrylic acid and its potential applications. Polym Bull 74:4659–4679. https://doi.org/10.1007/s00289-017-1981-7

Dashairya L, Rout M, Saha P (2018) Reduced graphene oxide - coated cotton as an efficient absorbent in oil-water separation. Adv Compos Hybrid Mater 1:1–14. https://doi.org/10.1007/s42114-017-0019-9

Dong ST, Zhou CH, Yan L, Yu H, Guo FZ, Wei HY (2010) Adsorption of acid red G dye on octadecyl trimethylammonium montmorillonite. Appl Clay Sci 50:427–431. https://doi.org/10.1016/j.clay.2010.08.018

Ennigrou DJ, Ali MBS, Dhahbi M (2014) Copper and zinc removal from aqueous solutions by polyacrylic acid assisted-ultrafiltration. Desalination 343:82–87. https://doi.org/10.1016/j.desal.2013.11.006

Hamidian AH, Atashgahi M, Khorasani N (2014) Phytoremediation of heavy metals (Cd, Pb and V) in gas refinery wastewater using common reed (Phragmitis australis). J Mater Chem 20:3079–3083. https://doi.org/10.1039/b925753e

Hu C, Deng Y, Hu H, Duan Y, Zhai K (2016) Adsorption and intercalation of low and medium molar mass chitosans on/in the sodium montmorillonite. Int J Biol Macromol 92:1191–1196. https://doi.org/10.1016/j.ijbiomac.2016.08.007

Hua J (2015) Synthesis and characterization of bentonite based inorgano–organo-composites and their performances for removing arsenic from water. Appl Clay Sci 114:239–246. https://doi.org/10.1016/j.clay.2015.06.005

Hua M, Zhang S, Pan B, Zhang W, Lv L, Zhang Q (2012) Heavy metal removal from water/wastewater by nanosized metal oxides: a review. J Hazard Mater 211-212:317–331. https://doi.org/10.1016/j.jhazmat.2011.10.016

Ijagbemi CO, Baek MH, Kim DS (2009) Montmorillonite surface properties and sorption characteristics for heavy metal removal from aqueous solutions. J Hazard Mater 166:538–546. https://doi.org/10.1016/j.jhazmat.2008.11.085

Jin M, Long M, Su H, Pan Y, Zhang Q, Wang J, Zhou B, Zhang Y (2017) Magnetically separable maghemite/montmorillonite composite as an efficient heterogeneous Fenton-like catalyst for phenol degradation. Environ Sci Pollut Res Int 24:1926–1937. https://doi.org/10.1007/s11356-016-7866-8

Li Y, Fang Z, Chen H, Zhang Y, Xu C, Chung KH, Shi Q (2015) Molecular characterization and transformation of dissolved organic matter in refinery wastewater from water treatment processes: characterization by Fourier transform ion cyclotron resonance mass spectrometry. Energ Fuel 29:151022093726008–151022093726963. https://doi.org/10.1021/acs.energyfuels.5b01446

Long H, Wu P, Zhu N (2013) Evaluation of Cs^+ removal from aqueous solution by adsorption on ethylamine-modified montmorillonite. Chem Eng J 225:237–244. https://doi.org/10.1016/j.cej.2013.03.088

Nicolás AM, Baltazar SE, Alejandra G, Daniela MOL, Pamela S, Rubio MA, Dora A (2016) Nanoscale zero valent supported by zeolite and montmorillonite: template effect of the removal of lead ion from an aqueous solution. J Hazard Mater 301:371–380. https://doi.org/10.1016/j.jhazmat.2015.09.007

Pawar RR, Lalhmunsiama BHC, Lee SM (2016) Activated bentonite as a low-cost adsorbent for the removal of Cu(II) and Pb(II) from aqueous solutions: batch and column studies. J Ind Eng Chem 34:213–223. https://doi.org/10.1016/j.jiec.2015.11.014

Ren X, Zhang Z, Luo H, Hu B, Dang Z, Yang C, Li L (2014) Adsorption of arsenic on modified montmorillonite. Appl Clay Sci 97-98:17–23. https://doi.org/10.1016/j.clay.2014.05.028

Wang J, Long MC, Zhang ZJ, Chi LN, Qiao XL, Zhu HX, Zhang ZF (2008) Removal of organic compounds during treating printing and dyeing wastewater of different process units. Chemosphere 71:195–202. https://doi.org/10.1016/j.chemosphere.2007.10.001

Wang Q, Chang X, Li D, Hu Z, Li R, He Q (2011) Adsorption of chromium(III), mercury(II) and lead(II) ions onto 4-aminoantipyrine immobilized bentonite. J Hazard Mater 186:1076–1081. https://doi.org/10.1016/j.jhazmat.2010.11.107

Wang G, Zhang S, YuyanHua SX, Ma S, Wang J, Tao Q, Wang Y, Komarneni S (2017) Phenol and_or Zn^{2+}, adsorption by single- or dual-cation organomontmorillonites. Appl Clay Sci 140:1–9. https://doi.org/10.1016/j.clay.2017.01.023

Wu P, Dai Y, Long H, Zhu N, Li P, Wu J, Dang Z (2012) Characterization of organo-montmorillonites and comparison for Sr(II) removal: equilibrium and kinetic studies. Chem Eng J 191:288–296. https://doi.org/10.1016/j.cej.2012.03.017

Ying YU, Liu B (2014) Absorption of Pb^{2+} from printing and dyeing wastewater with modified reed as absorbent. J Eastern Liaoning Univ 21:81–86. https://doi.org/10.14168/j.issn.1673-4939.2014.02.006

Yu X, Wei C, Lin K, Yun H, Xie X, Wu H (2010) Development of organovermiculite-based adsorbent for removing anionic dye from aqueous solution. J Hazard Mater 180:499–507. https://doi.org/10.1016/j.jhazmat.2010.04.059

Yu G, Lu Y, Guo J, Patel M, Bafana A, Wang X, Qiu B, Jeffryes C, Wei S, Guo Z (2018) Carbon nanotubes, graphene, and their derivatives for heavy metal removal. Adv Compos Hybrid Mater 1:56–78. https://doi.org/10.1007/s42114-017-0004-3

Zhang M, Chang L, Zhao Y, Yu Z (2018a) Fabrication, characterization and adsorption behavior of montmorillonite/polypyrrole nanocomposites for eosin Y removal. Polym Bull 75:1–19. https://doi.org/10.1007/s00289-018-2303-4

Zhang Y, Yan X, Yan Y, Chen D, Huang L, Zhang J, Ke Y, Tan S (2018b) The utilization of a three-dimensional reduced graphene oxide and montmorillonite composite aerogel as a multifunctional agent for wastewater treatment. RSC Adv 8:4239–4248. https://doi.org/10.1039/C7RA13103H

Zhou Q, Zhu R, Parker S, Zhu J, He H, Molinari M (2015) Modelling the effects of surfactant loading level on the sorption of organic contaminants on organoclays. RSC Adv 5:47022–47030. https://doi.org/10.1039/C5RA05998D

Zhu J, Yang J, Deng B (2010) Ethylenediamine-modified activated carbon for aqueous lead adsorption. Environ Chem Lett 8:277–282. https://doi.org/10.1007/s10311-009-0217-y

Zhu R, Chen Q, Zhou Q, Xi Y, Zhu J, He H (2016) Adsorbents based on montmorillonite for contaminant removal from water: a review. Appl Clay Sci 123:239–258. https://doi.org/10.1016/j.clay.2015.12.024